Excellent performance of Pt-C/TiO_2 for methanol oxidation: Contribution of mesopores and partially coated carbon

Xinbing Wu[a], Wei Zhuang*[,a, b], Linghong Lu*[, a], Licheng Li[a, c], Jiahua Zhu[d], Liwen Mu[d], Wei Li[e], Yudan Zhu[a] and Xiaohua Lu*[, a]

[a]*State Key Laboratory of Materials-Oriented Chemical Engineering, Nanjing Tech University, 5# Xinmofan Road, Nanjing 210009, PR China*

[b]*College of Biotechnology and Pharmaceutical Engineering, Nanjing Tech University, 30# Puzhu South Road, Nanjing 211816, PR China*

[c]*College of Chemical Engineering, Nanjing Forest University, 159# Longpan Road, Nanjing 210037, PR China*

[d]*Department of Chemical & Biomolecular Engineering, The University of Akron, Akron, OH 44325-3906, USA*

[e]*Chemical Engineering and Applied Chemistry & European Bioenergy Research Institute, Aston University, Aston Triangle Birmingham B4 7ET, UK*

*To whom correspondence should be addressed.

Contact information:

Dr. Wei Zhuang

Email: zhuangwei726@126.com

Prof. Linghong Lu

E-mail: linghonglu@njtech.edu.cn

Prof. Xiaohua Lu

E-mail: xhlu@njtech.edu.cn

Abstract: Partial deposition of carbon onto mesoporous TiO_2 (C/TiO_2) were prepared as supporting substrate for Pt catalyst development. Carbon deposition is achieved by in-situ carbonization of furfuryl alcohol. The hybrid catalysts were characterized by XRD, Raman, SEM and TEM and exhibited outstanding catalytic activity and stability in methanol oxidation reaction. The heterogeneous carbon coated on mesoporous TiO_2 fibers provided excellent electrical conductivity and strong interfacial interaction between TiO_2 support and Pt metal nanoparticles. Methanol oxidation reaction results showed that the activity of Pt-C/TiO_2 is 3.0 and 1.5 times higher than that of Pt-TiO_2 and Pt-C, respectively. In addition, the Pt-C/TiO_2 exhibited a 6.7 times enhanced stability compared with Pt-C after 2000 cycles. The synergistic effect of C/TiO_2 is responsible for the enhanced activity of Pt-C/TiO_2, and its excellent durability could be ascribed to the strong interfacial interaction between Pt nanoparticles and C/TiO_2 support.

Keywords: Mesoporous; Pt nanoparticles; Interfacial interaction; TiO_2; Carbon; Methanol oxidation

Introduction

Supporting material plays an important role in developing high performance catalysts, since the structure and surface property of catalyst support greatly influence the size and dispersion quality of metal nanoparticles [1-3]. The stability and durability of electrocatalysts have become the most challenging part in developing practically useful catalysts [4-6]. Metal oxide substrates have attracted great attention due to their high corrosion resistance and strong interactions with metal catalyst particles that could effectively prevent the agglomeration of metal particles [7, 8]. Moreover, and abundant hydroxyl groups on the surface could prevent the adsorption of CO-like intermediate species in electrocatalytic methanol oxidation reaction (MOR), and hence improve reaction stability [9-11]. Among the versatile metal oxides, TiO_2 has been extensively investigated as the support of fuel cell catalyst because of its natural abundance, low cost, environmental friendliness and high stability in fuel cell environment[12-14]. However, TiO_2 itself would not be used as electrocatalyst support unless its surface area could be dramatically increased and electrical conductivity could be imparted [15, 16].

Mesoporous TiO_2 fibers with the extralarge surface area and high crystallinity has been synthesized using a novel template-free method in our group [17]. And the mesoporous structure of TiO_2 would provide a confined micro-environment for the stabilization of highly dispersed metal nanoparticles [18]. Hybrid TiO_2-carbon materials have been employed to improve the conductivity of TiO_2 [2, 19, 20]. These hybrid materials may possess both electron conductivity of carbon and corrosion resistance of the metal oxide, and even a synergistic effect such as Pt and Ru [21, 22]. Gedanken [2] and Lee [23] prepared a core-shell structured composites with TiO_2 particles as cores and carbon as shell. The uniform and thin carbon shell is demonstrated to be effective to provide good electrical conductivity as well as excellent interfacial interaction between Pt nanoparticles and carbon [24, 25]. Shahgaldi [26] synthesized TiO_2-C core-shell structure and TiO_2 encapsulated in carbon nanospheres as a Pt support, and Pt-TiO_2-C depicted a relatively high activity

in electrocatalytic reaction [26]. Most of the reported work on carbon coated TiO_2 were processed with full coverage, which might cause some potential issues. First of all, when TiO_2 was fully covered by carbon, advantages of TiO_2 were reduced or covered as well. Secondly, the interfacial interaction between Pt nanoparticles and TiO_2 is weak, which would cause unstable and worse dispersion for Pt nanoparticles. Thirdly, the structure of carbon could collapse under low pH, high temperature and high potential work conditions, which may cause Pt nanoparticles detachment, agglomeration and sintering [27]. At last, Pt supported on carbon could be easily poisoned by the adsorbed CO-like intermediate species generated during methanol oxidation process [28, 29].

In order to obtain a durable and stable catalyst, we need fabricate a catalyst support with heterogeneous surface exposing both carbon and TiO_2 surfaces. In this work, we designed and prepared a novel structure of partially deposited carbon-TiO_2 composite (C/TiO_2) with mesoporous TiO_2 nanofibers as core and partially coated carbon as shell. Pt nanoparticles were deposited onto the support ($Pt\text{-}C/TiO_2$) afterwards with homogenously dispersed Pt nanoparticles on carbon, TiO_2 and C/TiO_2 interface. It is anticipated that the as-prepared $Pt\text{-}C/TiO_2$ exhibits outstanding catalytic stability and activity than that of Pt-C (Vulcan XC72 as support) and $Pt\text{-}TiO_2$ in MOR.

2 Experimental Section

2.1 Preparation of samples

Mesoporous TiO_2. Mesoporous TiO_2 has been synthesized with a simple template-free approach [17, 30]. Typically, 5.43 g of K_2CO_3 (reagent grade) and 12.67 g of $TiO_2 \cdot nH_2O$ (TiO_2 content: 47.24%) were mixed uniformly and sintered in a muffle oven at 810 °C for 2 h. Then 10.0 g of the product was soaked in 6.67 mL distilled water at 25 °C for 7 days. The resultant product was suspended in 1000 mL of 0.5 M HCl solution to exchange K^+ by H^+ with vigorously stirring. The product was filtered and washed with distilled water and dried in a desiccator at 60 °C under vacuum. The dried sample was heated to 500 °C for 2 h in a muffle oven to obtain TiO_2.

C/TiO_2 composite. C/TiO_2 composite was prepared as follows: 0.023 g of oxalic acid (OA) was added into 0.39 mL of furfuryl alcohol (FA) to obtain OA-FA solution. 1.0 g of TiO_2 was added into the OA-FA solution and stirred for 1 h at 25 °C, a light yellow sample was obtained. Then the sample was heated at 80 °C for 16 h in an oven to induce polymerization of the furfuryl alcohol. And the sample's color turned from light yellow to brown. The sample was heated to 800 °C with a heating rate 2 °C/min and then furtherly carbonized for 3 h under N_2 atmosphere to yield C/TiO_2. The carbon content is calculated as 15.2% based on thermogravimetric analysis.

Pt-C/TiO_2 catalyst. Pt-C/TiO_2 catalyst was prepared as follows: 12.52 mL of 1 M NaOH-ethylene glycol (EG) solution was added into H_2PtCl_6-EG solution (0.1594 g, 0.3077 mM in 50 mL) with stirring for 1 h to obtain a transparent yellow colloidal solution. Then the solution was heated at 163 °C for 4 h with a N_2 flow passing through the reaction system to evaporate water and organic byproducts. A transparent dark-brown homogeneous colloidal solution of the Pt metal nanocluster was obtained without any precipitate. Then 63.0 mL of 0.2 M HCl and 0.30 g of C/TiO_2 composite were dropped into the system and continuously stirred for another 10 hours. After that,

the C/TiO_2 supported Pt NPs can be obtained by filtering, washing and drying at 60 °C, and the product is named Pt-C/TiO_2. For comparison, commercial carbon black (Vulcan XC72) and TiO_2 were loaded with platinum following the same procedure, noted as Pt-C and Pt-TiO_2, respectively. The actual loading of Pt was determined by ICP-OES. The Pt content was 17.65%, 17.32% and 16.02% for Pt-TiO_2, Pt-C/TiO_2 and Pt-C, respectively.

2.2 Physical Characterization

The carbon content of the sample was determined using a thermogravimetric analyzer (Netzsch TG 209 F3, Germany) under O_2 atmosphere. The textural properties were studied by N_2 adsorption-desorption measurements (TriStarII 3020 M) at a liquid nitrogen temperature of 196 °C. The crystal phases of samples were determined by powder X-ray diffraction (XRD, Bruker D8, Cu 65 Kα radiation). The morphology of the composites was characterized by scanning electron microscopy (FESEM, Leo 1530 FEG SEM), and transmission electron microscopy (TEM, Philips Tecnai G2 20 S-TWIN at 200kV). TEM samples were prepared by depositing a drop of diluted suspension in ethanol on a lacey-film-coated copper grid. And the size of Pt nanoparticles was summarized 300 particles of each sample. The carbon fine structure of the specimen was determined using a Raman spectrometer (Jobin Yvon HR800 UV). The platinum content of the hybrid composites was measured by inductively coupled plasma optical emission spectrometry (ICP-OES, Optima2000DV, USA).

2.3 Electrochemical measurement

All the electrochemical measurements were carried out on an electrochemical workstation Autolab 302 N with a three-electrode system, which consisted of a glassy carbon working electrode, Pt gauze counter electrode, and Ag/AgCl (saturated KCl) reference electrode. 1.0 mg catalyst was dispersed ultrasonically in mixture containing 0.45 mL ethanol, 0.45 ml water and 100 μL Nafion solution (5 wt%) to obtain a homogeneous suspension. 20 μL of the resulting solution was uniformly pipetted onto the glassy carbon electrode and dried gently under air flow. To measure the methanol oxidation reaction activity, cyclic voltammograms (CVs) were recorded in a 1 M

CH_3OH/ 0.5 M H_2SO_4 aqueous solution. To study the catalyst stability, CVs were measured for 2000 cycles in a 0.5 M H_2SO_4 aqueous solution. The electrochemical active specific surface areas (ECSA) of platinum with coulombic charges accumulated during hydrogen desorption after correcting for the double-layer charging current from the CVs can be calculated[31, 32]:

$$ECSA = \frac{Q_H}{0.21 \times M_{Pt}}$$

where Q_H (mC) is the charge due to the hydrogen adsorption/desorption in the hydrogen region of the CVs, 0.21 mC□cm^{-2} is the electrical charge associated with monolayer adsorption of hydrogen on Pt, and M_{Pt} is the loading of Pt metal on the working electrode. The electrolytes were deaerated with ultrahigh purity N_2 for 30 min to remove the dissolved O_2 prior to the measurements.

3 Results and discussion

3.1 Characterization of the C/TiO₂ sample

The XRD patterns of TiO_2 and C/TiO_2 are presented in Fig.1 (a). Both TiO_2 and C/TiO_2 composite exhibit similar characteristic diffraction peaks, which index to the anatase phase of TiO_2 (JCPDS 21-1272) with high crystallinity. Lower crystallinity of TiO_2 is observed in the C/TiO_2 composite after carbonization as shown by the prominent characteristic diffraction peaks due to the carbon covered on the TiO_2[33]. There are no typical peaks of graphite, indicating the carbon in C/TiO_2 is amorphous. The Raman spectroscopy is a very useful tool to study the carbon phase in the composites. Raman spectra (Fig. 1 (b)) confirm the presence of the carbon in C/TiO_2. The characteristic G-band peak at ~1580 cm^{-1} and a D-band peak at ~1340 cm^{-1} represent the graphitic and amorphous carbon in both C/TiO_2 and Vulcan XC72[34].

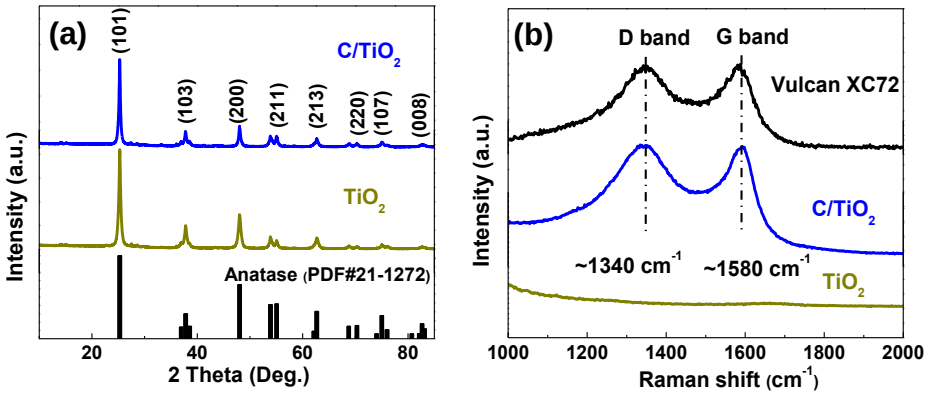

Fig. 1 (a) XRD patterns of TiO_2 and C/TiO_2; (b) Raman spectra of TiO_2, C/TiO_2 and Vulcan XC72.

Nitrogen adsorption-desorption isotherm was performed to determine the Brunauer-Emmett-Teller (BET) surface area. As shown in Fig. 2(a), TiO_2 and C/TiO_2 have similar type IV isotherms with a hysteresis loop, indicating the presence of well-developed mesopores in both two samples. Also, it can be seen that carbon doesn't completely block the mesopores of TiO_2, which is essentially important for

the stabilization of Pt NPs and efficient reactant transfer during reaction[35]. The BET surface area of C/TiO_2 increases to 157 $m^2 \cdot g^{-1}$, which is larger than that of pure TiO_2 (108 $m^2 \cdot g^{-1}$).The enlarged surface area is definitely beneficial to the dispersion of Pt NPs.

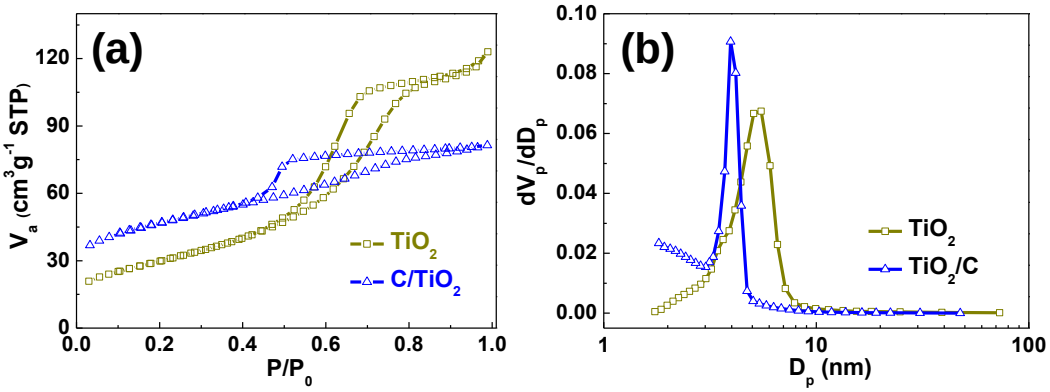

Fig. 2 (a) N_2 adsorption-desorption isotherms of TiO_2, C/TiO_2; (b) pore size distribution curves of samples.

The microstructure of TiO_2 and C/TiO_2 is depicted in Fig. 3. TiO_2 has a fiber-like morphology and smooth surface with a uniform width of 50~150 nm, Fig. 3(a). The morphology and structure of the mesoporous TiO_2 is further investigated by TEM (Fig. 3(b)). TEM image of an individual fiber shows numerous 5~10 nm bright spots correspond to the pores of the TiO_2, which is consistent with the BET results. Corresponding to the pore sizes, we speculate TiO_2 nanofibers arrange along the longitudinal direction where 10~30 nm wide nanocrystals build up the brick-like and mesoporous framework. After carbonization, the C/TiO_2 composite in Fig. 3(c) is shown to preserve the original morphology of the TiO_2 nanofibers and have a rough surface, which is assumed to be carbon coating on the TiO_2 surface. It is clear that uneven carbon network wrapped around TiO_2 fiber with thickness of 10~15 nm. According to the density of carbon (1.8 $g \cdot cm^{-3}$), and carbon content (15.2%, determined by TG measurement), we estimated that about 45% of the surface area of TiO_2 nanofibers are covered by carbon.

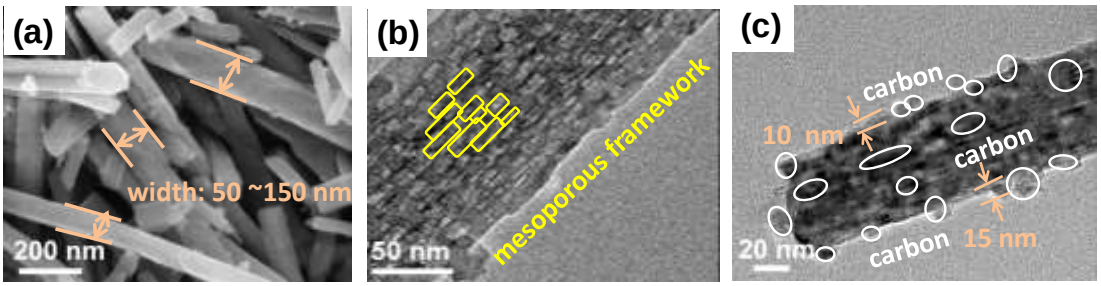

Fig. 3 (a) FESEM images of TiO_2; (b) TEM images of TiO_2; (c) TEM images of C/TiO_2.

3.2 Characterization of the C/TiO_2 sample modified with Pt

The XRD patterns of $Pt\text{-}C/TiO_2$ and Pt-C are presented in Fig. 4. Compared to the XRD pattern of C/TiO_2, the diffraction peaks of the face-centered-cubic (fcc) Pt lattice are clearly recognizable, as indicated by the characteristic peaks around 39.8, 46.8, 67.6, and 81.3° due to Pt (111), Pt (200), Pt (220), and Pt (311), respectively. This indicates that the Pt nanoparticles are composed of pure crystalline Pt [36, 37]. The diffraction peak for Pt (220) is used to estimate the Pt NPs size with the Scherrer equation, because there is no interference from other diffraction peaks, and the average size of $Pt\text{-}C/TiO_2$ and Pt-C is about 2.1 nm and 2.5 nm, respectively[38].

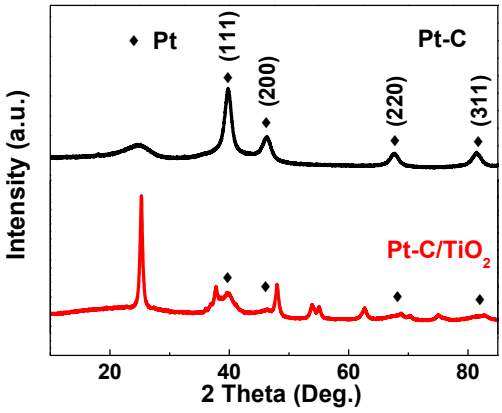

Fig. 4 XRD patterns of $Pt\text{-}C/TiO_2$ and Pt-C

TEM images of Fig. 5(a,b) show the morphology and structure of $Pt\text{-}C/TiO_2$. It is obivous from the $Pt\text{-}C/TiO_2$ TEM images (Fig. 5(a)) that Pt NPs with a mean particle size of 2.0±0.5 nm are well dispersed on the surface of C/TiO_2 without discernible aggregation, which is desirable in an efficient electrocatalyst. $Pt\text{-}TiO_2$ interface shown

in the HRTEM image in Fig. 5(b) gives the lattice spacing of 0.19 and 0.20 nm for TiO_2 support and Pt, respectively. This lattice-matched interface leads to a compact Pt-TiO_2 interface that can stabilize the imbedded Pt NPs. In addition, TEM image of Pt-C shows that the size of Pt NPs is 2.5±1.0 nm in Fig. 5(c).

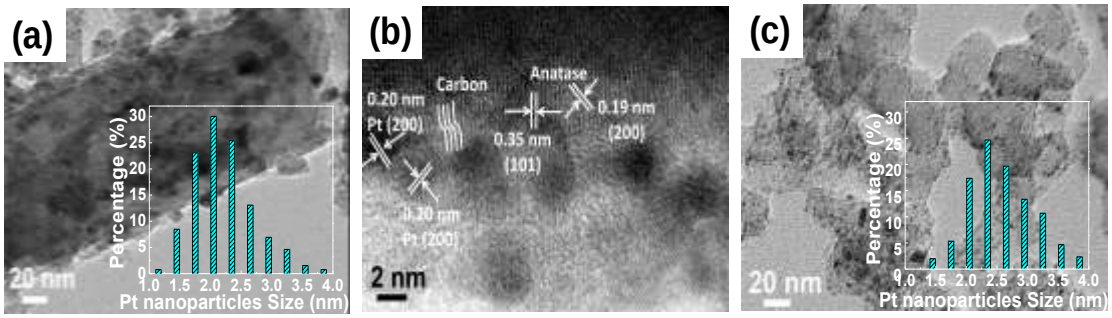

Fig. 5 (a) TEM images of Pt-C/TiO_2, inset: size distribution of Pt NPs on C/TiO_2; (b) HRTEM images of Pt-C/TiO_2; (c) TEM images of Pt-C, inset: size distribution of Pt NPs on Vulcan XC72.

3.3. Electrochemical properties

In order to investigate the electrocatalytic activity of the Pt-C/TiO_2 composites and Pt-C, the cyclic voltametric measurements of methanol oxidation were carried out in 1.0 M CH_3OH /0.5 M H_2SO_4 solution at room temperature at a scan rate of 50 mV/s (Fig. 6). The current density of the methanol oxidation peak is largest with Pt-C/TiO_2 (1.22 mA□cm^{-2}) (Table 1), which is 3.0 and 1.5 times higher than those of Pt-TiO_2 (0.41 mA□cm^{-2}) and Pt-C (0.82 mA□cm^{-2}), respectively.

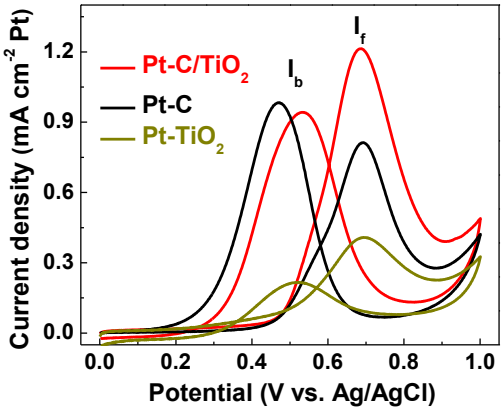

Fig. 6 Cyclic voltammograms of methanol electrooxidation in 1 M CH_3OH/0.5 M H_2SO_4, scan rate: 50 mV/s.

The forward anodic peaks at around 0.70 V are due to methanol oxidations, and in the backward scan the oxidation peaks at about 0.53 V can be attributed to the oxidations of adsorbed CO or CO-like species[39]. During the reverse scan, CO-like adspecies can be oxidized by Pt-OH_{ads} in the acidic electrolyte within the potential range where the reverse anodic peak develops[40]. If the maximum peak current density in the forward is designated as I_f and the maximum peak current density in the backward is designated as I_b, the ratio of I_f/I_b is generally used to evaluate the tolerance of the catalysts to incompletely oxidized species accumulated on the surface of the electrode[11, 41]. A higher ratio of I_f/I_b represents more complete methanol oxidation, less accumulation of CO or CO-like species on the catalyst surface, and thus a better CO-tolerance. In contrast, a lower I_f/I_b ratio implies the reverse results. The I_f/I_b ratio for Pt-TiO_2 (1.9) and Pt-C/TiO_2 (1.3) composites are larger than that for Pt-C (0.83), which suggests that the support of TiO_2 catalyst leads to more complete methanol oxidation and less accumulation of CO-like species than that of carbon and leads to a higher resistance to CO poisoning in the MOR. This result can be linked to the high poison tolerance to CO-like intermediates and good electrochemical stability of Pt-C/TiO_2 catalyst. Additionally, this can furthermore be ascribed to the strong interaction between Pt and support and a possible bifunctional effect between Pt nanoparticles and TiO_2, which is similar with the commonly accepted bifunctional mechanism of methanol electro-oxidation between Pt and Ru [42, 43]. Dissociative adsorption of water molecules on the TiO_2 support creates TiO_2-OH surface groups. TiO_2-OH groups adjacent to Pt nanoparticles may readily oxidize CO groups bonded on the peripheral Pt atoms, of which the electronic structure is greatly modified by the TiO_2 support[9].

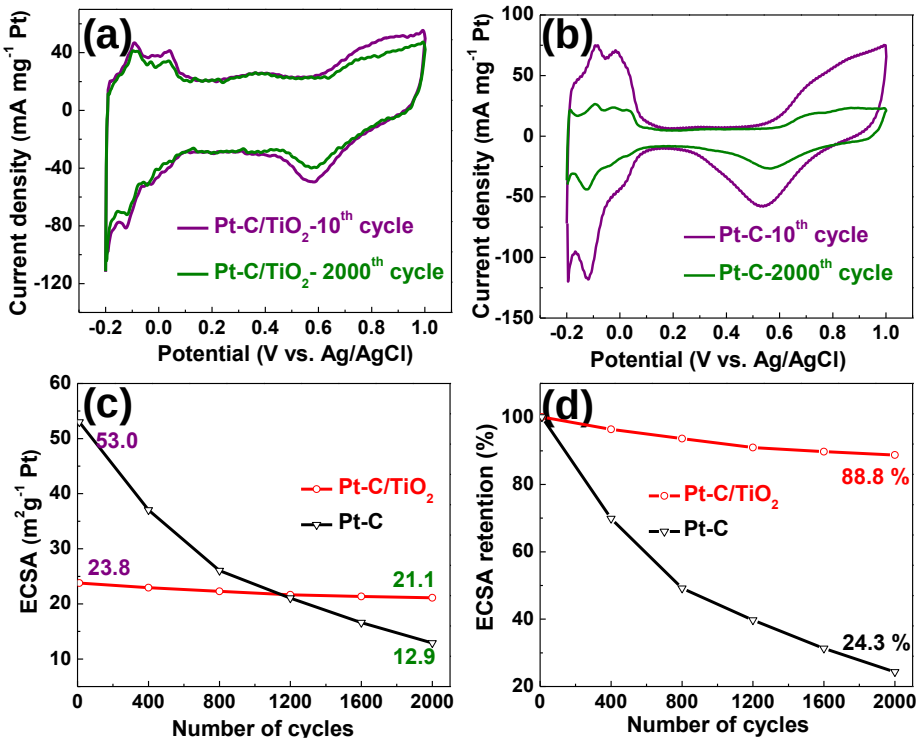

Fig. 7 (a, b) Cyclic voltammograms of Pt-C/TiO_2 and Pt-C after 10 and 2000 cycles in 0.5 M H_2SO_4, scan rate = 100 mV/s; (c) ECSAs of samples as a function of the number of CVs, (d) ECSA retention as a function of the number of cycles.

Catalyst stability was investigated by monitoring electrochemical active surface area during extended cyclic voltammograms cycling tests. The ECSA of the Pt catalyst was estimated based on the hydrogen desorption peaks observed between -0.02 and 0.15 V vs. Ag/AgCl. A hydrogen desorption charge of 0.21 mC□cm^{-2} was assumed for ECSA calculation[32]. The CVs shown in Fig. 7 (a, b) indicate that ECSA of both Pt-C/TiO_2 and Pt-C decrease after 2000 continuous cycles in 0.5 M H_2SO_4 solution. The active Pt area of the commercial carbon-supported catalyst measured after the first 10 cycles (53.0 m^2 g^{-1}) is higher than that of the C/TiO_2-supported catalyst (23.8 m^2 g^{-1}). However, after 2000 cycles, the ECSA of Pt-C (12.9 m^2 g^{-1}) is much smaller than that of Pt-C/TiO_2 (21.1 m^2 g^{-1}). The trends of ECSA change are plotted in Fig. 7(c.d). C/TiO_2-supported catalyst is more stable than carbon-supported catalyst because 88.8% of the ECSA of Pt-C/TiO_2 is still available while only 24.3% of ECSA of Pt-C remains after 2000 cycles. The Pt-C/TiO_2 catalyst is approximately 6.7 times more stable than the Pt-C catalyst, which could be

attributed to the mesoporous structure of C/TiO_2 support and the interaction between Pt NPs and TiO_2 surface. In addition, voltammetric measurements performed with the carbon-supported catalyst yields a peak at 0.52 V for the cathodic sweep (Fig. 7(b)). After 2000 cycles, the peak at 0.52 V is reduced to a shoulder, and a subtle peak remains at 0.57 V. Therefore, these cathodic features located at 0.52 and 0.57 V may represent the reduction of platinum oxide and interaction with functional groups on the carbon surface, respectively[44]. The decrease in the platinum oxide reduction peak implies a significant loss of Pt active sites after 2000 cycles.

Table 1 Activity and stability of various catalysts.

Sample	Specific I_{peak} ($mA\ cm^{-2}$ Pt)	E_{peak} (V)	I_f/I_b	$ECSA_{10}^{th}$ ($m^2\ g^{-1}$)	$ECSA_{2000}^{th}$ ($m^2\ g^{-1}$)	ECSA Retention	Ref.
Pt-TiO_2	0.41	0.692	1.88	9.0	/	/	This work
Pt-C/TiO_2	1.22	0.688	1.29	23.8	21.1	88.8%	This work
Pt-C	0.82	0.694	0.83	53.0	12.9	24.3%	This work
Pt/CCT	0.69	0.91	0.77	198	/	/	[2]
Pt/C	0.37	0.98	0.96	95	/	/	[2]
Pt/ TiO_2-rGO	1.05	0.685	1.17	31	/	/	[45]
Pt/TiO_2-3h	0.19	0.59	1.44	172.9	/	/	[21]
Pt/C	0.83	0.66	1.08	24	/	/	[28]
Pt-(WC/C)	0.83	0.69	1.21	81	/	/	[28]
Pt/CNT	0.57	0.84	0.89	79	/	/	[33]
Pt/TiO_2	/	0.77	1.21	/	/	/	[33]
Pt/CNT/TiO_2	0.60	0.81	0.99	40	/	/	[33]
Pt/RGO1	0.25	0.70	2.73	43	/	/	[38]
Pt/RGO2	0.27	0.69	2.21	38	/	/	[38]
Pt/RGO3	0.24	0.72	2.62	55	/	/	[38]
Pt/C	0.35	0.68	1.30	24	/	/	[38]
Pt/CCG	/	0.69	0.83	36	/	/	[39]
Pt/MWCNT	/	0.67	0.72	33	/	/	[39]

Fig. 8(a, b) shows TEM images of Pt-C/TiO_2 and Pt-C catalysts after 2000 CV cycles in 0.5 M H_2SO_4. The size distribution of Pt particles is summarized from four images of each sample and shown in the Fig. 8 (c, d). The change of size distribution from 2.5±1.0 nm to 4.0±1.5 nm indicates that Pt NPs on carbon agglomerated and became larger. Size distribution of the Pt NPs on C/TiO_2 exhibits the minor change from 2.0±0.5 nm to 2.3±0.5 nm, which is a convincing evidence of enhanced stability of Pt NPs on C/TiO_2. It is well known that the properties of metal-support composites are strongly dependent on the metal particle size and dispersion. Normally, a smaller particle size results in better catalytic performance but easier agglomeration [46]. The decrease of ECSA of Pt-C can be attributed to the observation from the size change and losing of Pt NPs. Therefore, the mesoporous structure and the heterogeneous interface of C/TiO_2 help to enhance the stability of Pt on the C/TiO_2 surface**.**

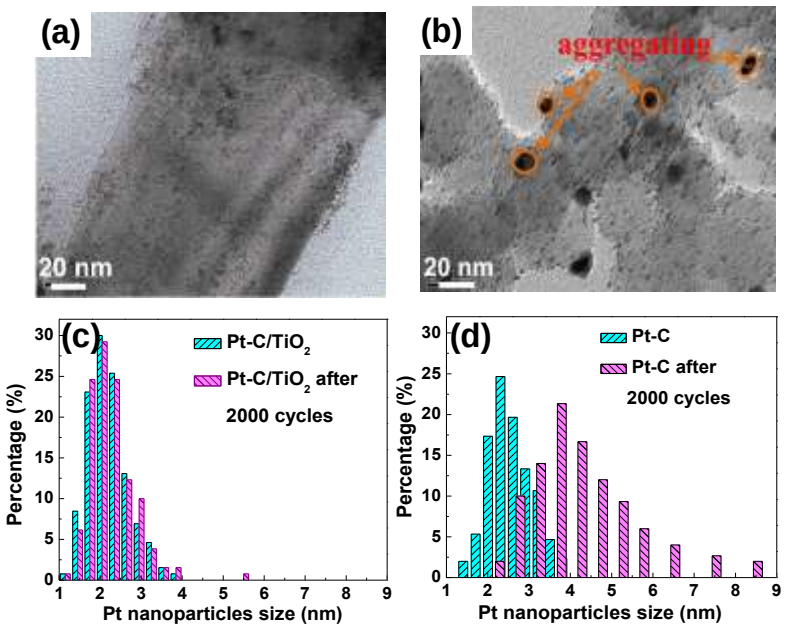

Fig. 8 (a, b) TEM images of Pt-C/TiO_2 (a) and Pt-C (b) after 2000 cycles, (c,d): size distribution of Pt NPs corresponding to each change in catalysts.

4 Conclusions

We designed and prepared a carbon-TiO_2 composite as Pt support, which with mesoporous TiO_2 as core and partially coated carbon as shell to fully utilize the combined advantages of both materials. Electrochemical and structural

characterization clearly demonstrated that Pt nanoparticles catalyst supported on C/TiO_2 showed enhanced activity and stability in the methanol oxidation reaction. The methanol oxidation activity of Pt-C/TiO_2 was 3.0 and 1.5 times higher than that of Pt/TiO_2 and Pt-C, respectively. Pt-C/TiO_2 was 6.7 times more stable than Pt-C after 2000 cycles. Carbon network wrapped around mesoporous TiO_2 offers good electronic conductivity while partially exposed TiO_2 retains its advantages such as good stability and the strong metal-support interaction.

Acknowledgments

This work was financially supported by the Major Research Plan of the National Natural Science Foundation of China (91334202), the Key Project of National Natural Science Foundation of China (21136004), the National Natural Science Foundation of China (21176113, 21506090), and the Natural Science Foundation of the Jiangsu Higher Education Institutions of China (14KJB530008).

References

[1] G.S. Chai, S.B. Yoon, J.H. Kim, J.-S. Yu, Spherical carbon capsules with hollow macroporous core and mesoporous shell structures as a highly efficient catalyst support in the direct methanol fuel cell, Chem. Commun., (2004) 2766-2767.

[2] S. Shanmugam, A. Gedanken, Carbon-coated anatase TiO2 nanocomposite as a high-performance electrocatalyst support, Small, 3 (2007) 1189-1193.

[3] W.X. Huang, G.H. Sun, C. Tian, Surface chemistry of group IB metals and related oxides, Chem. Soc. Rev., 46 (2017) 1977-2000.

[4] M.K. Debe, Electrocatalyst approaches and challenges for automotive fuel cells, Nature, 486 (2012) 43-51.

[5] L. Lin, W. Zhou, R. Gao, S. Yao, X. Zhang, W. Xu, S. Zheng, Z. Jiang, Q. Yu, Y.-W. Li, Low-temperature hydrogen production from water and methanol using Pt/α-MoC catalysts, Nature, 544 (2017) 80-83.

[6] W. Huang, H. Wang, J. Zhou, J. Wang, P.N. Duchesne, D. Muir, P. Zhang, N. Han, F. Zhao, M. Zeng, J. Zhong, C. Jin, Y. Li, S.-T. Lee, H. Dai, Highly active and durable methanol oxidation electrocatalyst based on the synergy of platinum–nickel hydroxide–graphene, Nat. Commun., 6 (2015) 8.

[7] S. Yao, X. Zhang, W. Zhou, R. Gao, W. Xu, Y. Ye, L. Lin, X. Wen, P. Liu, B. Chen, Atomic-layered Au clusters on α-MoC as catalysts for the low-temperature water-gas shift reaction, Science, (2017).

[8] F. Xiong, Y.Y. Yu, Z.F. Wu, G.H. Sun, L.B. Ding, Y.K. Jin, X.Q. Gong, W.X. Huang, Methanol Conversion into Dimethyl Ether on the Anatase TiO2(001) Surface, Angew. Chem.-Int. Edit., 55 (2016) 623-628.

[9] C.S. Chen, F.M. Pan, Electrocatalytic activity of Pt nanoparticles deposited on porous TiO2 supports toward methanol oxidation, Appl. Catal. B-Environ., 91 (2009) 663-669.

[10] Z. Zhang, J. Liu, J. Gu, L. Su, L. Cheng, An overview of metal oxide materials as electrocatalysts and supports for polymer electrolyte fuel cells, Energy & Environmental Science, 7 (2014) 2535-2558.
[11] H. An, G.-H. An, H.-J. Ahn, Octahedral Co3O4/carbon nanofiber composite-supported Pt catalysts for improved methanol electrooxidation, Journal of Alloys and Compounds, 645 (2015) 317-321.
[12] Y. Ma, X.L. Wang, Y.S. Jia, X.B. Chen, H.X. Han, C. Li, Titanium Dioxide-Based Nanomaterials for Photocatalytic Fuel Generations, Chem. Rev., 114 (2014) 9987-10043.
[13] M. Cao, D. Wu, R. Cao, Recent Advances in the Stabilization of Platinum Electrocatalysts for Fuel-Cell Reactions, ChemCatChem, 6 (2014) 26-45.
[14] W. Zhuang, L.H. Lu, X.B. Wu, W. Jin, M. Meng, Y.D. Zhu, X.H. Lu, TiO2-B nanofibers with high thermal stability as improved anodes for lithium ion batteries, Electrochem. Commun., 27 (2013) 124-127.
[15] Y.H. Qin, Y.F. Li, R.L. Lv, T.L. Wang, W.G. Wang, C.W. Wang, Enhanced methanol oxidation activity and stability of Pt particles anchored on carbon-doped TiO2 nanocoating support, J. Power Sources, 278 (2015) 639-644.
[16] S.K. Das, M. Patel, A.J. Bhattacharyya, Effect of Nanostructuring and Ex situ Amorphous Carbon Coverage on the Lithium Storage and Insertion Kinetics in Anatase Titania, ACS Appl. Mater. Interfaces, 2 (2010) 2091-2099.
[17] M. He, X.H. Lu, X. Feng, L. Yu, Z.H. Yang, A simple approach to mesoporous fibrous titania from potassium dititanate, Chem. Commun., (2004) 2202-2203.
[18] Y. Bai, W. Li, C. Liu, Z.H. Yang, X. Feng, X.H. Lu, K.Y. Chan, Stability of Pt nanoparticles and enhanced photocatalytic performance in mesoporous Pt-(anatase/TiO2(B)) nanoarchitecture, J. Mater. Chem., 19 (2009) 7055-7061.
[19] X. Yan, Y.J. Li, F. Du, K. Zhu, Quan, A. Su, G. Chen, Y. Wei, Synthesis and optimizable electrochemical performance of reduced graphene oxide wrapped mesoporous TiO2 microspheres, Nanoscale, 6 (2014) 4108-4116.
[20] Y. Lai, W. Liu, J. Li, K. Zhang, F. Qin, M. Wang, J. Fang, High performance sodium storage of Fe-doped mesoporous anatase TiO2/amorphous carbon composite, Journal of Alloys and Compounds, 666 (2016) 254-261.
[21] C.-S. Chen, F.-M. Pan, Electrocatalytic activity of Pt nanoparticles deposited on porous TiO2 supports toward methanol oxidation, Applied Catalysis B: Environmental, 91 (2009) 663-669.
[22] K. Drew, G. Girishkumar, K. Vinodgopal, P.V. Kamat, Boosting Fuel Cell Performance with a Semiconductor Photocatalyst: TiO2/Pt−Ru Hybrid Catalyst for Methanol Oxidation, The Journal of Physical Chemistry B, 109 (2005) 11851-11857.
[23] J.M. Lee, S.B. Han, J.Y. Kim, Y.W. Lee, A.R. Ko, B. Roh, I. Hwang, K.W. Park, TiO2@carbon core-shell nanostructure supports for platinum and their use for methanol electrooxidation, Carbon, 48 (2010) 2290-2296.
[24] D.Y. Chung, K.-J. Lee, Y.-E. Sung, Methanol Electro-Oxidation on the Pt Surface: Revisiting the Cyclic Voltammetry Interpretation, The Journal of Physical Chemistry C, 120 (2016) 9028-9035.
[25] F.M. Rhen, C. McKeown, Enhanced Methanol Oxidation on Strained Pt Films, The Journal of Physical Chemistry C, 121 (2017) 2556-2562.
[26] S. Shahgaldi, J. Hamelin, Stability study of ultra-low Pt thin film on TiO2–C core–shell structure and TiO2 encapsulated in carbon nanospheres as cathode catalyst in PEMFC, Fuel, 150 (2015) 645-655.
[27] K. Sasaki, M. Shao, R. Adzic, Dissolution and Stabilization of Platinum in Oxygen Cathodes, in: F.N.

Büchi, M. Inaba, T.J. Schmidt (Eds.) Polymer Electrolyte Fuel Cell Durability, Springer New York, New York, 2009, pp. 7-27.
[28] C.a. Ma, L. Kang, M. Shi, X. Lang, Y. Jiang, Preparation of Pt-mesoporous tungsten carbide/carbon composites via a soft-template method for electrochemical methanol oxidation, Journal of Alloys and Compounds, 588 (2014) 481-487.
[29] T. Huang, S. Mao, G. Zhou, Z. Zhang, Z. Wen, X. Huang, S. Ci, J. Chen, A high-performance catalyst support for methanol oxidation with graphene and vanadium carbonitride, Nanoscale, 7 (2015) 1301-1307.
[30] W. Li, C. Liu, Y.X. Zhou, Y. Bai, X. Feng, Z.H. Yang, L.H. Lu, X.H. Lu, K.Y. Chan, Enhanced Photocatalytic Activity in Anatase/TiO2(B) Core−Shell Nanofiber, The Journal of Physical Chemistry C, 112 (2008) 20539-20545.
[31] Z.Z. Jiang, Z.B. Wang, Y.Y. Chu, D.M. Gu, G.P. Yin, Ultrahigh stable carbon riveted Pt/TiO2-C catalyst prepared by in situ carbonized glucose for proton exchange membrane fuel cell, Energy & Environmental Science, 4 (2011) 728-735.
[32] A. Pozio, M. De Francesco, A. Cemmi, F. Cardellini, L. Giorgi, Comparison of high surface Pt/C catalysts by cyclic voltammetry, J. Power Sources, 105 (2002) 13-19.
[33] Z.I. Bedolla-Valdez, Y. Verde-Gómez, A.M. Valenzuela-Muñiz, Y. Gochi-Ponce, M.T. Oropeza-Guzmán, G. Berhault, G. Alonso-Núñez, Sonochemical synthesis and characterization of Pt/CNT, Pt/TiO2, and Pt/CNT/TiO2 electrocatalysts for methanol electro-oxidation, Electrochim. Acta, 186 (2015) 76-84.
[34] Z.M. Luo, L.H. Yuwen, B.Q. Bao, J. Tian, X.R. Zhu, L.X. Weng, L.H. Wang, One-pot, low-temperature synthesis of branched platinum nanowires/reduced graphene oxide (BPtNW/RGO) hybrids for fuel cells, J. Mater. Chem., 22 (2012) 7791-7796.
[35] D. He, Y. Rong, Z. Kou, S. Mu, T. Peng, R. Malpass-Evans, M. Carta, N.B. McKeown, F. Marken, Intrinsically microporous polymer slows down fuel cell catalyst corrosion, Electrochem. Commun., 59 (2015) 72-76.
[36] Y.Y. Mu, H.P. Liang, J.S. Hu, L. Jiang, L.J. Wan, Controllable Pt nanoparticle deposition on carbon nanotubes as an anode catalyst for direct methanol fuel cells, J. Phys. Chem. B, 109 (2005) 22212-22216.
[37] A. Liu, M. Yuan, M. Zhao, C. Lu, T. Zhao, P. Li, W. Tang, Graphene modulated assembly of PtPd bimetallic catalysts for electro-oxidation of methanol, Journal of Alloys and Compounds, 586 (2014) 99-104.
[38] S. Sharma, A. Ganguly, P. Papakonstantinou, X. Miao, M. Li, J.L. Hutchison, M. Delichatsios, S. Ukleja, Rapid Microwave Synthesis of CO Tolerant Reduced Graphene Oxide-Supported Platinum Electrocatalysts for Oxidation of Methanol, J. Phys. Chem. C, 114 (2010) 19459-19466.
[39] Y.J. Li, W. Gao, L.J. Ci, C.M. Wang, P.M. Ajayan, Catalytic performance of Pt nanoparticles on reduced graphene oxide for methanol electro-oxidation, Carbon, 48 (2010) 1124-1130.
[40] J. Prabhuram, R. Manoharan, Investigation of methanol oxidation on unsupported platinum electrodes in strong alkali and strong acid, J. Power Sources, 74 (1998) 54-61.
[41] Z.H. Wen, Q. Wang, J.H. Li, Template synthesis of aligned carbon nanotube arrays using glucose as a carbon source: Pt decoration of inner and outer nanotube surfaces for fuel-cell catalysts, Adv. Funct. Mater., 18 (2008) 959-964.
[42] F. Liu, J.Y. Lee, W.J. Zhou, Segmented Pt/Ru, Pt/Ni, and Pt/RuNi nanorods as model bifunctional catalysts for methanol oxidation, Small, 2 (2006) 121-128.

[43] J.H. Chen, M.Y. Wang, B. Liu, Z. Fan, K.Z. Cui, Y.F. Kuang, Platinum Catalysts Prepared with Functional Carbon Nanotube Defects and Its Improved Catalytic Performance for Methanol Oxidation, The Journal of Physical Chemistry B, 110 (2006) 11775-11779.
[44] F. Gao, R. Thomann, C.E. Nebel, Aligned Pt-diamond core-shell nanowires for electrochemical catalysis, Electrochem. Commun., 50 (2015) 32-35.
[45] W. Zhuang, L. He, J. Zhu, R. An, X. Wu, L. Mu, X. Lu, L. Lu, X. Liu, H. Ying, TiO2 nanofibers heterogeneously wrapped with reduced graphene oxide as efficient Pt electrocatalyst supports for methanol oxidation, Int. J. Hydrog. Energy, 40 (2015) 3679-3688.
[46] S.I. Sanchez, L.D. Menard, A. Bram, J.H. Kang, M.W. Small, R.G. Nuzzo, A.I. Frenkel, The Emergence of Nonbulk Properties in Supported Metal Clusters: Negative Thermal Expansion and Atomic Disorder in Pt Nanoclusters Supported on gamma-Al2O3, J. Am. Chem. Soc., 131 (2009) 7040-7054.